ELSEVIER

Journal of Hazardous Materials 49 (1996) 57–88

JOURNAL OF HAZARDOUS MATERIALS

Monitoring and modeling of PCB dry deposition in urban area

Wen-Jhy Lee [a,*], Chun-Ching Su [a], Hwey-Lin Sheu [a], Yi-Chin Fan [a], How-Ran Chao [a], Guor-Cheng Fang [b]

[a] *Department of Environmental Engineering, National Cheng Kung University, Tainan 70101, Taiwan*
[b] *Department of Industrial Safety and Hygiene, Hungkuang Institute of Medical and Nursing Technology, Taichung 43309, Taiwan*

Received 2 July 1995; accepted 14 November 1995

Abstract

Dry deposition and air sampling were undertaken simultaneously in the ambient air of an urban site by using several dry deposition plates, two MOUDIs (micro-orifice uniform deposited impactors), one NRI (Noll rotary impactor) and several PS-1 (General Metal Work, PS-1) samplers from January to May 1994 in Tainan City, Taiwan. The dry deposition plate, which had a smooth surface, was always pointed into the wind. The PCB (polychlorinated biphenyl) congeners were analyzed primarily by using a gas chromatograph with a ^{63}Ni electron capture detector (ECD). The measured dry deposition flux of total PCBs varied between 3.48 and 6.79 $\mu g\ m^{-2}$ per day and averaged $\approx 4.73\ \mu g\ m^{-2}$ per day. This was up to three orders of magnitude higher than the fluxes measured at the Great Lake and remote areas and close to those measured at urban areas by previous studies. The particle-bound PCB homologue composition collected by the dry deposition plate varied between 0.76 $\mu g\ g^{-1}$ (di-CBs) and 11.5 $\mu g\ g^{-1}$ (hexa-CBs). This profile of PCB homologues is similar to the pattern of Aroclor 1260 which is dominant in hexa-CBs and hepta-CBs. Because of their higher vapor pressure, in general, the less-chlorinated PCB homologues have a greater PCB mass fraction in the gas phase. The mean dry deposition velocities of PCB homologues ranged between 0.09 and 0.58 cm s^{-1}. In general, the more highly chlorinated PCB homologues have a higher dry deposition velocity. Particle size distributions ($dC/d(\log D_p)$ vs. D_p) of total PCBs were found to be bimodal. The highest peak was localized in the particle size range between 5.6 and 10.0 μm and the second peak was localized in the particle size range between 0.31 and 0.52 μm. The particle MMD_0 of total PCBs was 1.68 μm and more than 85% of the PCB mass was found in the particles smaller than 10 μm. By using the particle size distribution data, the dry deposition model used in this study can provide a good prediction for the dry deposition flux of total particle mass, total PCBs and PCB homologues. For both total

* Corresponding author.

SSDI 0304-3894(95)00159-X

particle mass and total PCBs, more than 87.5% of the dry deposition flux is contributed by particles of size > 10 μm. This is because particles larger than 10 μm have a higher dry deposition velocity (> 2.60 cm s^{-1}) and, therefore, control the majority of the dry deposition flux.

Keywords: Ambient air; Dry deposition; Modeling; Particle size distribution; Polychlorinated biphenyl; Urban

1. Introduction

Dry deposition is an important pathway for the transfer of semi-volatile compounds from air to land and water. Interest in atmospheric deposition has increased over the past decade because of concerns about the effects of the deposited material entering the environment and its subsequent health effects.

The process of dry deposition includes three steps: aerodynamic transport, boundary layer transport, and interactions with the receptor surface. The first step involves contaminant transport from the free atmosphere down to the quasi-laminar sublayer immediately adjacent to the surface. Movement across the sublayer comprises boundary layer transport, and physical and chemical interactions between the contaminant and the surface material make up the final transport step [1].

Polychlorinated biphenyls (PCBs) have a heavy oil-like consistency, high boiling points, a high degree of chemical stability, low flammability and low electrical conductivity. Because of the above characteristics, PCBs are used primarily in transformers and capacitors as the dielectric fluid and in a variety of other applications. The ability of PCBs to volatilize from sources and to resist degradation at low incinerating temperatures makes atmospheric transport the primary mode of global distribution. PCBs exhibit lipophilic and hydrophobic properties in water and therefore are found to be accumulated in lipid layers of biota. As PCB-containing products are used widely in urban areas, the PCB concentration in the ambient air of urban areas is more than one order of magnitude higher than that in rural or remote areas [2–11].

Previous attempts to quantify PCB dry deposition have shown that there is still no generally acceptable technology for sampling and analyzing dry deposition flux. Therefore, until now, there have been insufficient data both to reliably estimate and to understand the movement of PCBs in the environment. The dry deposition flux can be measured by using a smooth plate with a sharp leading edge that is pointed into the wind by a wind vane. Its collection surface is patterned after those used in wind tunnel studies, because this provides minimum air flow disruption and thus provides an estimate of the lower limit for dry deposition flux [10,12].

The dry deposition of aerosol-containing semi-volatile organic compounds (SOCs) (such as PAH, PCB and PCDD/PCDF) in the ambient air onto a receptor surface depends on the type of surface characteristics, the properties of the deposited pollutant and the meteorological conditions [13]. Holsen et al. [10] measured the PCB dry deposition flux and showed that it is up to three orders of magnitude higher in urban areas than in nonurban areas. In addition, PCBs were found to be associated with particles, particularly with coarse particles, which represented a significant fraction of the total PCB dry deposition flux, even though PCBs in the ambient air were present primarily in the vapor phase [10].

Atmospheric dry deposition of PCBs into Lake Michigan has been estimated by Swackhamer and Armstrong [6] and by Doskey and Andren [3]; the high PCB concentrations in lake fish and precipitation even in pristine areas suggested the significance of atmospheric inputs. Eisenreich et al. [2] also studied the dry deposition of PCBs into the Great Lakes, concluding that atmospheric deposition fluxes of PCBs include a combination of dry and wet removal processes and that dry deposition is 1.5–5.0 times the wet deposition. Leister and Baker [14] estimated the atmospheric deposition of organic contaminants into Chesapeake Bay and found that the dry deposition flux of the tetrachlorobiphenyls contributes up to 35% of the total sum of the PCB atmospheric flux [14].

Koster and Hites [15] measured the dry deposition flux of polychlorinated dibenzo-*p*-dioxins and dibenzofurans (PCDD/PCDF). This was the first time that the dry deposition flux of PCDD/PCDF had been measured directly. The results of the study indicated that the dry deposition flux of PCDD/PCDF increased as the temperature decreased and also that the efficiency of removal by dry deposition for PCDD/PCDF increased with increasing levels of chlorination [15].

The differences between dry deposition velocities may be due to differences in the experimental procedures employed, in the physical properties of the compounds investigated, and in the methodologies used for the estimation [16]. McMahon and Denison [17] reported that deposition velocity is an approximately linear function of wind speed and friction velocity. By solving the mass balance equation under selected conditions, Bidleman and Christensen [18] concluded that a higher dry deposition velocity was observed for the less volatile PCBs. The results of a study by Swackhamer et al. [7] showed that the dry deposition velocity for PCBs into Siskiwit Lake was 0.16 cm s^{-1} and that the wet deposition was generally three times as great as dry deposition and was dominated by particle washout.

As a significant fraction of PCB flux is likely to be deposited into land and water, the estimated total flux of PCBs may be significantly underestimated because of the high concentrations of PCBs that exist in the ambient air of urban areas. In this study, dry deposition and air sampling were undertaken, simultaneously, in the ambient air of an urban site with several dry deposition plates, two MOUDIs (micro-orifice uniform deposited impactors), one NRI (Noll rotary impactor) and several PS-1 samplers from January to May 1994 in Tainan City, Taiwan, to characterize the PCB dry deposition in urban area. The dry deposition flux and ambient air concentration and also the size distribution of PCBs and the total particle mass were measured. Then the dry deposition velocity and dry deposition flux of both PCBs and total particle mass contributed by each particle size range were calculated, and are discussed below.

2. Experimental section

2.1. Sampling program

Urban site samples were taken on the roof of a four-story (13 m height) building located in a mixed institutional, commercial, and residential area in the center of Tainan

Table 1
Sampling information for dry deposition plate, PS-1 sampler, wind speed and atmospheric temperature

Sampling no.	Sampling period (1994)	Exposure time for dry deposition plate (days)	Sampling volume for PS-1 sampler (m^3)	Mean wind Speed ($m\ s^{-1}$)	Atmospheric temperature (°C)
1	1/21–2/2	6.9	1188	0.90	16
2	2/19–2/26	6.0	931	0.74	19
3	3/28–4/3	6.4	932	0.80	22
4	4/25–4/30	5.0	941	0.53	29
5	5/16–5/25	5.0	943	0.56	29

City, Taiwan. The building is approximately 900 m away from a bus station. During periods of no rain or no threat of rain, the dry deposition plates allow adequate material to be deposited for the PCB analysis. Each set of dry deposition plate samples was typically exposed for 4–7 days. During each sampling period, several 24-h PS-1, MOUDI and NRI samples were obtained and composed, respectively, to carry out the

Table 2
Sampling information for MOUDI and NRI

No.	Sampling period (1994)	Sampler		Sampling volume (m^3)
1	1/21–2/2	NRI:	6 Stage	440.0
			B Stage	1319.9
			C Stage	3959.6
			D Stage	3959.6
		MOUDI		260.7
2	2/19–2/26	NRI:	A Stage	262.7
			B Stage	788.1
			C Stage	2364.3
			D Stage	2364.3
		MOUDI		346.0
3	3/28–4/3	NRI:	A Stage	349.1
			B Stage	1047.4
			C Stage	3142.1
			D Stage	3142.1
		MOUDI		375.8
4	4/25–4/30	NRI:	A Stage	334.0
			B Stage	1002.0
			C Stage	3005.9
			D Stage	3005.9
		MOUDI		418.9
5	5/16–5/25	NRI:	A Stage	452.9
			B Stage	1358.9
			C Stage	4076.6
			D Stage	4076.6
		MOUDI		535.3

PCB analysis and to determine the mean PCB concentration for the gas phase or for each particle size range. The sampling information is shown in Tables 1 and 2.

2.2. Dry deposition plate

The dry deposition flux was measured by using a smooth surface plate with a sharp leading edge, mounted on a wind vane [19]. The plate used in this study was similar to those used in wind tunnel studies [20]. It was made of polyvinyl chloride (PVC) and was 21.5 cm long, 8.0 cm wide and 0.8 cm thick with a sharp leading edge ($< 10°$ angle) that was pointed into the wind. In order to verify that there were no system mistakes during the experiments, five duplicate plate samples on a side by side basis were taken during each of the sampling periods.

Each of the plates was covered with aluminum strips (10 cm $\times$ 8 cm) coated with approximately 5 mg of silicon grease (thickness $\approx$ 1 μm) to collect impacted particles and gases (132 cm^2 of total exposed surface). This hydrophobic grease has a high molecular weight and low vapor pressure and is therefore suitable for measuring PCB flux. The film was placed on the plate and held down at the edges with a 0.3 mm thick stainless steel template, which was secured at each end by acrylic slats screwed into the plate. The plate was cut so that it would slide onto a 3 cm diameter rod. Two screws were fastened through the plate to a wind vane, allowing the plate to swing freely into the wind. Individual plates were separated by 55 cm (horizontally), which was shown experimentally to be sufficient to prevent sample interactions. The strips were weighed before and after sampling to determine the total mass of the particles collected. The strips were then extracted and analyzed for PCBs. Analysis of unexposed aluminum strips (blanks) showed that their PCB mass was below the detection limits of this study.

During the sampling periods, atmospheric particle and PCB mass size distributions were measured with two MOUDIs and a NRI. Then the complete atmospheric particle size distributions (from 0.056 to 100 μm) for total particle mass and PCBs were obtained.

2.3. MOUDI

The MOUDI is an 8-stage cascade impactor. Each stage on the MOUDI consists of an impaction plate for the nozzle plate above and a nozzle plate for the impaction plate below. The use of micro-orifice nozzles can extend the cut sizes of the lower stages to 0.05 μm without creating an excessive pressure drop across the impactor stages. Therefore, by rotating alternate stages of the MOUDI, deposits are distributed uniformly on the circular impaction areas $\approx$ 1 inch (25 mm) in diameter. The flow rate is 30 l min^{-1} and cut size diameters range from 10 μm at the first stage to 0.05 μm at the last [21].

Available cut size diameters were 10, 5.6, 3.2, 1.8, 1.0, 0.56, 0.32, 0.18 and 0.1 or 0.056 μm (choice of eight). A 15 μm pre-impactor is built into the inlet and this deposit is also available for analysis. The sample substrates are held to the impaction plate by removable clamping rings, and the entire impaction plate assemblies are held in place by magnets for easy removal. The base of the MOUDI holds an after-filter in a removable

filter holder similar to the impaction plates. Interchangeable impaction plates and filter holders are provided so that the impaction plate substrates and filters can be loaded and unloaded in the laboratory, decreasing the chance of damaging the particle deposits during in-the-field substrate removal. Sealed transport covers for impaction plates and filter holders are provided so that the impaction plates and after-filter can be transported to and from the test site without contamination. The sealed covers also minimize evaporative loss of samples during storage and chemical reaction with ambient gases [21].

2.4. Noll rotary impactor

The atmospheric coarse particle mass was measured with the NRI, which is well suited to collect the large particles that conventional samples exclude. It is a multi-stage rotary inertial impactor that collects coarse particles by simultaneously rotating four rectangular collectors (stages) of different dimensions through the air. The stages are covered with Mylar strips coated with silicon grease. Total collection areas were 1.2 cm^2, 3.1 cm^2, 10.3 cm^2 and 10.3 cm^2 for stages A, B, C, and D respectively. The strips were weighed before and after sampling to determine the particle mass collected. The NRI was operated for a maximum of 12 h before the Mylar strips were replaced.

In this study, the NRI was operated at 320 rpm, which produced theoretical aerodynamic cut diameters (assuming a particle density of 1 g cm^{-3}) of 6.5–100 μm, 11.5–100 μm, 24.7–100 μm and 36.5–100 μm for stages A, B, C, and D respectively. The volume of air samples for each stage of the NRI is calculated by multiplying the exposed surface area by its average rotational distance, its rotational speed (rpm), and the sampling time. The NRI is described in more detail in Refs. [22,23]. After combining the MOUDI and NRI, the normalized particle size ranges for each stage, in sequence, were 0.056–0.166, 0.166–0.31, 0.31–0.52, 0.52–1.0, 1.0–1.8, 1.8–3.2, 3.2–5.6, 5.6–10, 10–24.7, 24.7–36.5 and 36.5–100 μm, respectively.

2.5. Semi-volatile sampler

Ambient air samples for the total suspended particulate (TSP) and gas phase of PCBs were collected by using a standard semi-volatile sampling train (General Metal Works PS-1). The sampler, fitted with a glass fiber filter (cleaned by heating to 450°C), was weighed before and after sampling to determine the TSP collected. A glass cartridge containing a 5 cm polyurethane form (PUF) plug followed by a 2.5 cm XAD-2 resin and finally a 2.5 cm PUF plug cleaned by sequential extraction was used to collect the vapor phase PCBs. The glass fiber filters, PUF plugs and resin were stored and transported in clean screw-capped jars with Teflon cap liners. Glass fiber filters were transported to and from the field in prebaked glass plates and wrapped with aluminum foil.

2.6. PCB analysis

After final weighing, the PCB sample was placed in a solvent solution (a 1:1 v/v mixture of n-hexane and dichloromethane) and extracted in a Soxhlet extractor for 24 h.

Table 3
PCB congeners analyzed (IUPAC number grouped by homologue)

PCB homologue	Abbreviation	IUPAC number grouped by homologue
Dichlorobiphenyl	(Di-CBs)	4, 6, 7, 5+8, 15+18 [a]
Trichlorobiphenyl	(Tri-CBs)	17, 19, 22, 24+27, 25, 26, 28, 31, 32, 33
Tetrachlorobiphenyl	(Tetra-CBs)	41+71, 42, 44, 45, 46, 47, 48, 49, 52, 53, 54, 56+60, 63, 64, 67+100 [b], 70+76, 74, 66+80+95 [c]
Pentachlorobiphenyl	(Penta-CBs)	82, 83, 84, 85, 87, 89, 91, 97, 99, 101, 103, 105, 107, 110, 114, 118, 119
Hexachlorobiphenyl	(Hexa-CBs)	128, 129, 130, 131, 132, 134, 135, 136, 137, 138, 141, 144, 146, 149, 151, 153, 156, 158, 167
Heptachlorobiphenyl	(Hepta-CBs)	170+190, 171, 172, 173, 174, 175, 176, 177, 178, 180, 182+187, 183, 185, 189, 191, 193
Octachlorobiphenyl	(Octa-CBs)	194, 195, 196+203, 198, 197, 199, 200, 201, 205

[a] Half of 15+18 counted as Di, half counted as Tri.
[b] Half of 67+100 counted as Tetra, half counted as Penta.
[c] Two thirds of 66+80+95 counted as Tetra, one third counted as Penta.

The extract was then concentrated, cleaned up and reconcentrated to exactly 0.4 ml using a procedure similar to those described by Manchester-Neesvig and Andren [8].

The analysis of PCBs was conducted by using a Hewlett-Packard 5890A gas chromatograph (GC) equipped with a ^{63}Ni electron capture detector, an electronic pressure controller (EPC), a Hewlett-Packard capillary column (HP Ultra 2, 50 m × 0.32 mm × 0.17 μm), an HP-7673A automatic sampler and a computer workstation. The conditions for PCB analysis were as follow: splitless injection (300°C), volume of sample injected 2 μl, detector ECD operated at 280°C, oven 50–100°C at 3°C min^{-1}, 100–240°C at 0.6°C min^{-1}, and 240-290°C at 4°C min^{-1}, held at 270°C for 55 min. A 95% argon/5% methane mixture was used as the makeup gas.

The GC for PCB analysis was calibrated with a diluted equal-mass mixture of Aroclors 1242, 1248, 1254, and 1260. Concentrations of the individual congeners were calculated using the data in Ref. [8]. A mixture of 10 congeners was used to generate a correction curve to Mullin et al.'s relative retention time (RRT) data [24] for identification of individual congeners, similar to the method described by Manchester-Neesvig and Andren [8]. Specific PCB congeners identified, grouped by homologue and used in this study are shown in Table 3. Standards were injected daily to confirm retention times and response factors.

Analysis of serial dilutions of PCB standards found that the limit of detection was between 0.029 and 0.535 pg for individual congeners. The limit of quantification (LOQ) ranged between 6.1 and 117 pg m^{-2} per day for the dry deposition plate. Ten consecutive injections of a PCB standard yielded an average calculated error (standard deviation/average area) of 4.63% with a range of 1.13-11.6%. Recovery of internal standards—octachloronaphthalene (OCN) and tetrachloronaphthalene (TCN)—injected

into the extraction solvent averaged 91% and varied between 81 and 103%. Recovery of OCN applied directly to the aluminum strip of a dry deposition plate averaged 83% and varied between 76 and 90%.

PCB recovery efficiencies were determined by processing a solution containing known PCB concentrations through the same experimental procedure used for the samples. This study showed that the recovery efficiency of PCB congeners varied between 0.765 and 1.14 and averaged 0.854. The blank tests for PCBs were peformed by using the same procedure as the recovery efficiency tests without adding the known standard solution before extraction. Analyses of field blanks, including the blank samples used for MOUDI, NRI, PS-1 and dry deposition plates, found no significant contamination (GC integrated area below the detection limit). Analysis of duplicate experiments yielded differences in total PCB dry deposition flux varying between 11% and 23% and averaging 16%.

3. Results and discussion

3.1. Dry deposition flux of total PCBs and total particle mass

The measured dry deposition flux of total PCBs varied between 3.48 and 6.79 $\mu g\ m^{-2}$ per day and averaged $\approx 4.73\ \mu g\ m^{-2}$ per day (Fig. 1). It was higher in February

Table 4
Dry deposition flux of PCBs measured by previous studies

Compounds	Location	Value ($\mu g\ m^{-2}$ per day)	Reference
PCB homologues	Chesapeake Bay		Leister and Baker [14]
Trichloro		0.000721	
Tetrachloro		0.00134	
Pentachloro		0.000849	
Hexachloro		0.000575	
Heptachloro		0.000247	
Octachloro		0.0000822	
Nonachloro		0.0000110	
Total PCBs		0.00384	
PCB total	Chicago	2.800–9.700	Holsen et al. [10]
PCB total	Urban	0.274–1.918	Eisenreich et al. [2]
PCB total	Rural	0.137–1.370	Eisenreich et al. [2]
PCB total	Great Lake	0.055–0.411	Eisenreich et al. [2]
PCB total	Lake Superior	0.008	Baker and Eisenreich [9]
PCB total	Lake Michigan	0.0012–0.0024	Swackhamer and Armstrong [6]
PCB total	Lake Michigan	0.193	Doskey and Andren [25]
PCB total	Marine/Remote	0.0005–0.055	Eisenreich et al. [2]
PCB aerosol	Pinconning	0.0093–0.0247	McClure [26]

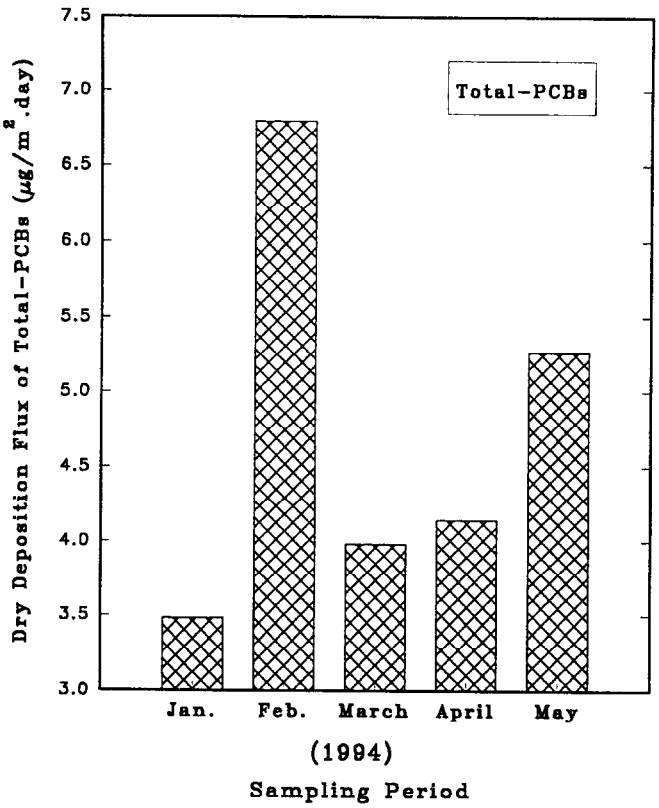

Fig. 1. Dry deposition flux of total PCBs.

and May and lower in January, March and April. No regular trend of total PCB dry deposition flux was found during these sampling periods. The PCB flux measured by previous studies is shown in Table 4. The PCB dry deposition flux measured in this study was up to three orders of magnitude higher than those measured at the Great Lakes and in remote areas and close to those measured in urban areas [2,4,6,7,10,11]. The differences may be influenced by the sources of the pollutants and the local meteorological conditions. Wind blowing from urban or industrial areas may carry higher concentrations of pollutants, resulting in a higher dry deposition flux of PCBs.

The measured dry deposition flux of total particle mass varied between 121 and 144 mg m^{-2} per day and averaged $\approx$ 134 mg m^{-2} per day (Fig. 2). This mean value (134 mg m^{-2} per day) was approximately 20% lower than that measured in the Chicago area which varied between 94.2 and 299 mg m^{-2} per day and averaged 171 mg m^{-2} per day [10,11]. The PCB mass deposited on the dry deposition plate and normalized by the total particle mass is designated the particle-bound PCB composition; it varied from 24.2 to 47.2 $\mu g\ g^{-1}$ and averaged 35.3 $\mu g\ g^{-1}$, which is the same level as that measured in Chicago [11].

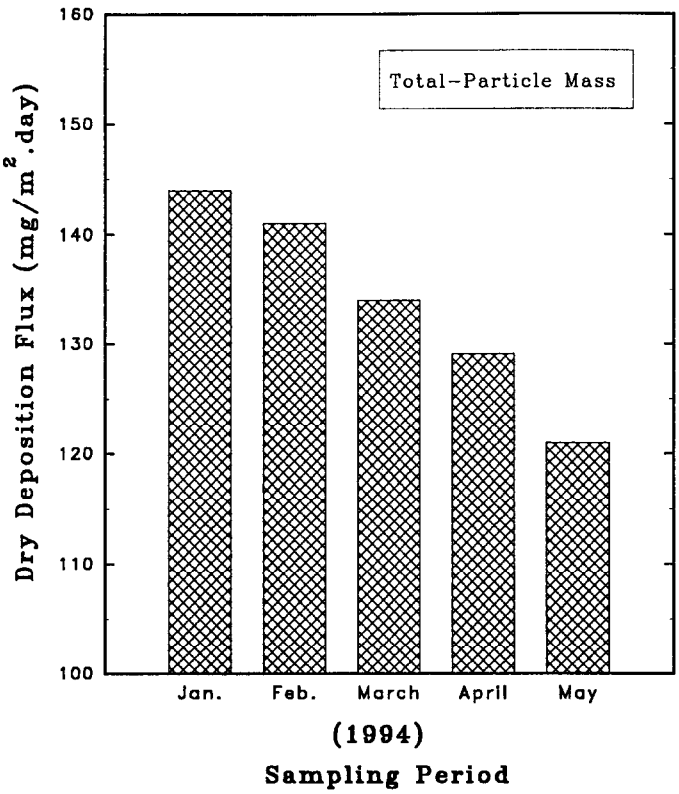

Fig. 2. Dry deposition flux of total particle mass.

3.2. Dry deposition flux of PCB homologues

The profiles of mean dry deposition flux of PCB homologues are shown in Fig. 3. In decreasing sequence, they were 1.54, 1.02, 0.75, 0.64, 0.35, 0.33 and 0.10 $\mu g\ m^{-2}$ per day for hexa-CBs, hepta-CBs, tetra-CBs, penta-CBs, octa-CBs, tri-CBs, and di-CBs, respectively. The particle-bound PCB composition collected by the dry deposition plate varied between 0.76 $\mu g\ g^{-1}$ (di-CBs) and 11.5 $\mu g\ g^{-1}$ (hexa-CBs) (Fig. 4). These profiles of PCB homologues are similar to the pattern of Aroclor 1260, which is dominant in hexa-CBs and hepta-CBs [8].

PCBs are semi-volatile organic compounds (SOCs). In the atmosphere, they exist in both the vapor and the particlate phase. With the same surface properties and meteorological conditions, the difference in dry deposition flux among PCB homologues is controlled mainly by their phase distributions, by their concentrations in the atmosphere and by particle size distributions. The measured phase distributions of PCB homologues are shown in Fig. 5. In general, the less-chlorinated PCB homologues have a higher PCB mass fraction in the gas phase: 86%, 73%, 65%, 58%, 43.7%, 42% and 44.7% for the

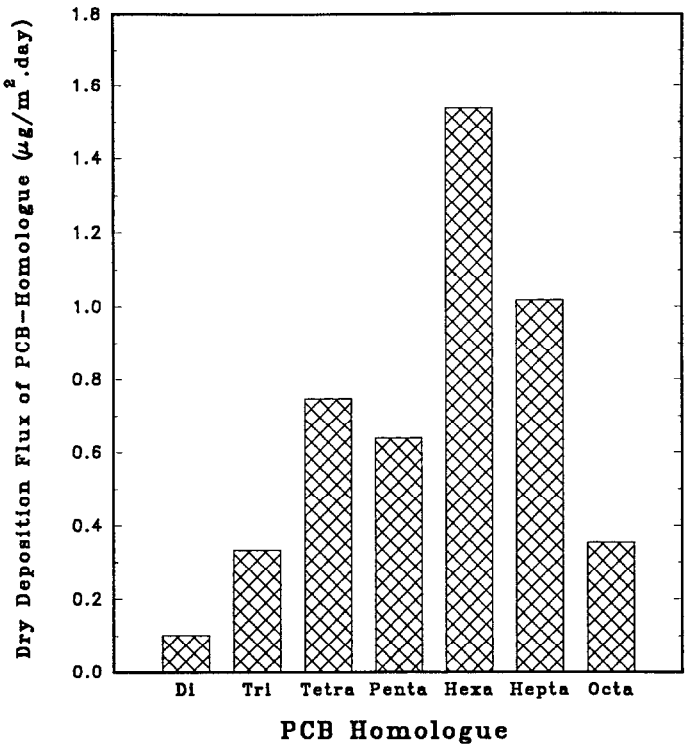

Fig. 3. Dry deposition flux of PCB homologues.

di-CBs, tri-CBs, tetra-CBs, hexa-CBs, hepta-CBs and octa-CBs, respectively. The measured phase distribution of hexa-CBs, hepta-CBs and octa-CBs is fairly constant.

3.3. Dry deposition velocities of total PCBs

The dry deposition velocities of PCBs were calculated as follows

$$V_{d,PCB} = K(F_T)/(C_g + C_p) \quad (1)$$

where $V_{d,PCB}$ is the dry deposition velocity of PCBs (cm s^{-1}); K is the transfer coefficient of units and equal to (1000 ng/μg) × (day/86 400 s) × (100 cm/m) or 1.1574074(ng/μg) × (day/s) × (cm/m); F_T is the dry deposition flux of PCBs (μg m^{-2} per day); C_g is the ambient air concentration of PCBs in the gas phase (ng m^{-3}); and C_f is the ambient air concentration of PCBs in the particulate phase (the summation of 11 stages) (ng m^{-3}).

The dry deposition velocities of total PCBs varied between 0.17 and 0.36 cm s^{-1} and averaged 0.28 cm s^{-1} (Fig. 6). The measured dry deposition velocities of total PCBs in this study were similar to the values measured or estimated by previous studies (Table 5).

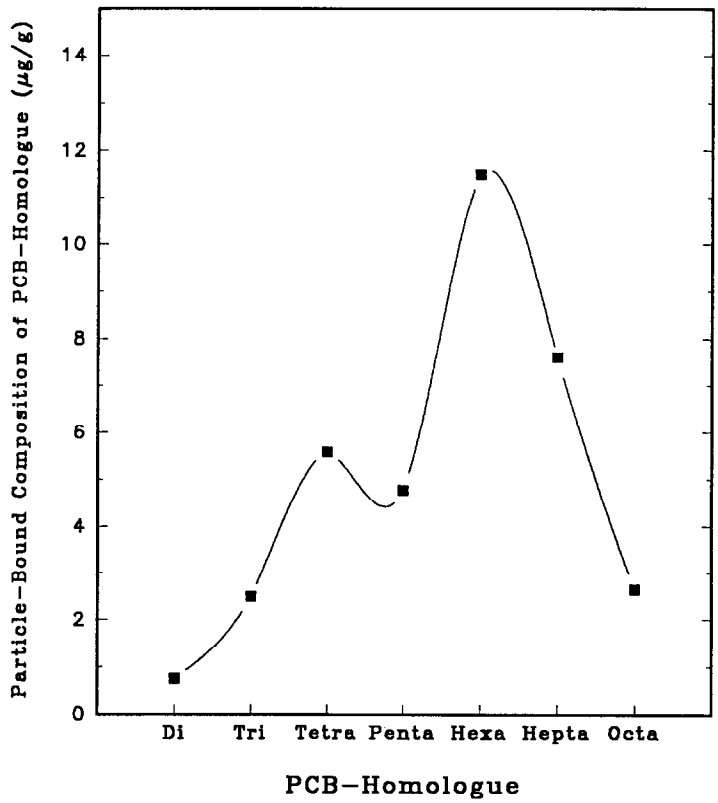

Fig. 4. Particle-bound composition of PCB homologues collected by the dry deposition plate.

Table 5
Dry deposition velocities V_d of PCBs measured by previous studies

Compounds	V_d (cm s^{-1})	Reference
PCB total	0.42	Lee [11]
PCB-1254	0.43	Bidleman and Christensen [18]
PCB-1254	0.50	Eisenreich et al. [4]
PCB-1242	0.50	Eisenreich et al. [4]
PCB-1016	0.038	Bidleman and Christensen [18]
PCB-1016	0.04	Eisenreich et al. [4]
PCB total	0.40	Eisenreich et al. [4]
PCB total	0.18	Atlas et al. [27]
PCB total	0.50	Doskey and Andren [25]
PCB total	0.50	Holsen et al. [10]
PCB total	0.16±0 13	Swackhamer et al. [7]
PCB aerosol	0.91	McClure [26]
PCB aerosol	0.49±0.23	Dolske and Sievering [28]

3.4. Dry deposition velocities of PCB homologues

The mean dry deposition velocities of PCB homologues were 0.09, 0.16, 0.23, 0.27, 0.58, 0.38 and 0.56 cm s^{-1} for di-, tri-, tetra-, penta-, hexa-, hepta- and octa-CBs, respectively (Fig. 7). In general, the dry deposition velocities increased as the levels of chlorination increased. This happens because the lower-chlorinated PCB homologues are enriched in the gas phase (Fig. 5). Dry deposition of gas phase PCBs is mainly by diffusion and involves lower dry deposition velocities. However, The more highly chlorinated PCB homologues primarily associated with the particle phase (Fig. 5) are deposited mostly by gravitational settling [10]. The dry deposition velocities produced by gravitational settling are much higher than those by diffusion [10].

3.5. Dry deposition modeling

The deposition velocities for atmospheric particles by the dry deposition model were obtained with the following equation [29]

$$V_d = V_{st} + 1.12U^* \exp(-30.36/D_p) \quad (2)$$

where V_{st} is the particle settling velocity (cm s^{-1}), U^* is the frictional velocity (cm s^{-1}), and D_p is the particle diameter (μm).

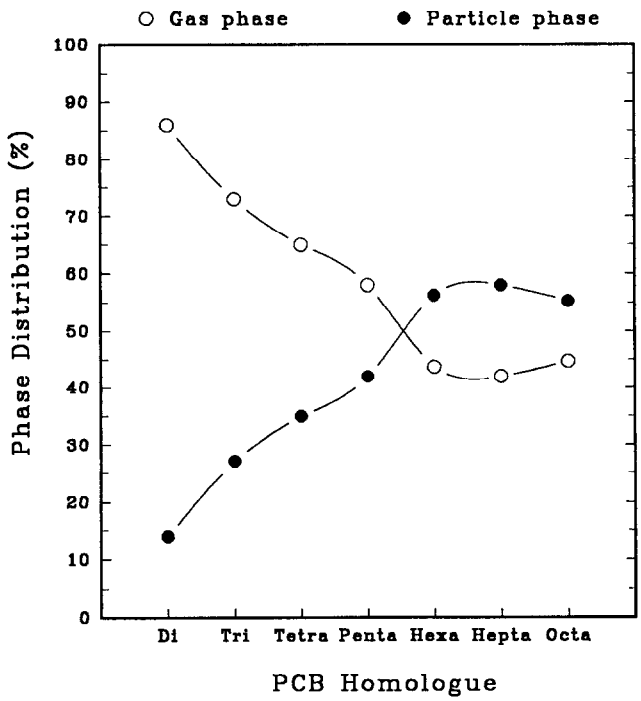

Fig. 5. Phase distribution of PCB homologues.

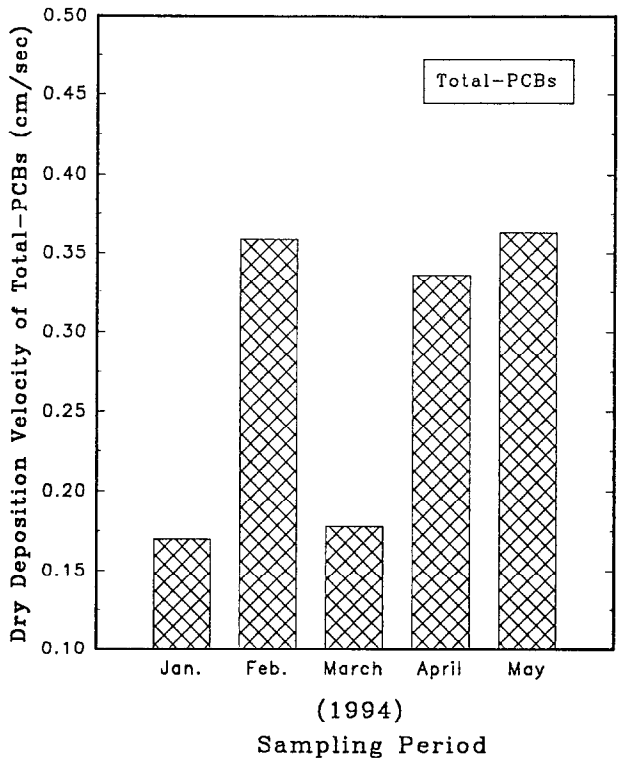

Fig. 6. Dry deposition velocity of total PCBs.

Two meteorological parameters that influence atmospheric turbulence are frictional velocity U^* and surface roughness Z_0. The relationship between these parameters for near neutral atmospheric stability conditions is

$$U = \frac{U^*}{k} \ln \frac{Z - d}{Z_0} \tag{3}$$

where U is the measured mean wind speed at height Z (cm s^{-1}), Z is the measured height above ground (m), k is von Karman's constant (0.4), d is the datum displacement (m), and Z_0 is the surface roughness height (m).

As the wind was measured at only one datum displacement, the average height of the structure surrounding the sampling site was taken as 8.0 m. A datum level displacement of 6.4 m (80% of the average structure height) was subtracted from the height (13 m) at which the wind speed was recorded. The roughness coefficient was estimated by the general relationship that Z_0 is approximately one thirtieth of the average roughness height. As the average height for the area surrounding the sampling site was 8.0 m, a roughness height of 0.27 m was used for calculating frictional velocity. The frictional velocities for wind speed measured in this study were calculated by using Eq. (3).

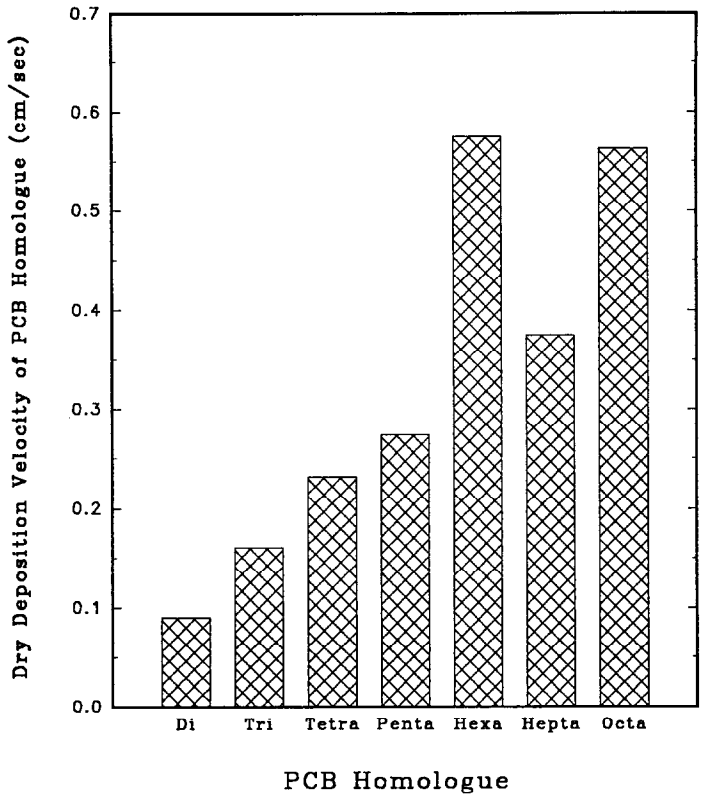

Fig. 7. Dry deposition velocity of PCB homologues.

The modeled $V_{d,i}$ values of individual impactor stages were 0.000092, 0.000286, 0.000716, 0.00209, 0.0065, 0.0198, 0.0695, 0.382, 2.61, 6.45 and 20.1 cm s^{-1} for the particle size ranges 0.056–0.166 (mean $D_p = 0.111$ μm), 0.166–0.31 (mean $D_p = 0.238$ μm), 0.31–0.52 (mean $D_p = 0.415$ μm), 0.52–1.0 (mean $D_p = 0.76$ μm), 1.0–1.8 (mean $D_p = 1.4$ μm), 1.8–3.2 (mean $D_p = 2.5$ μm), 3.2–5.6 (mean $D_p = 4.4$ μm), 5.6–10.0 (mean $D_p = 7.8$ μm), 10.0–24.7 (mean $D_p = 17.35$ μm), 24.7–36.5 (mean $D_p = 30.6$ μm) and 36.5–100 μm (mean $D_p = 68.25$ μm), respectively (Fig. 8). For each impactor stage, because the variation of wind speed was minor, during five sampling periods the variation of $V_{d,i}$ was fairly small.

3.6. Particle size distribution of total particle mass

The particle size distributions ($dC/d(\log D_p)$ vs. D_p) of total particle mass are shown in Fig. 9. Although the concentration ($dC/d\log D_p$) in the particle size range 0.52-1.8 μm was lower than those for the ranges 0.31-0.52 μm and 1.8-3.2 μm, the overall profile of Fig. 9 shows a unimodal distribution and the peak is localized at the particle size range of 0.31-3.2 μm. In Tainan city there is no significant industrial source for

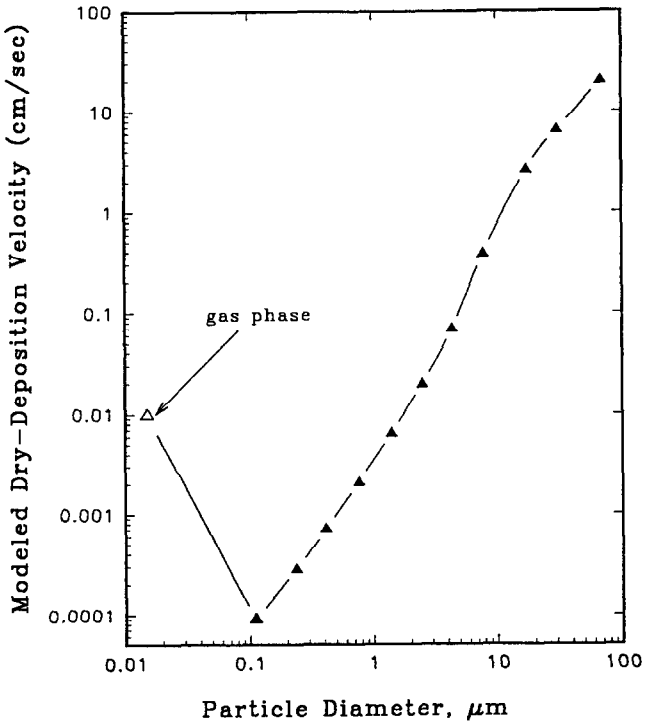

Fig. 8. Modeled dry deposition velocity vs. particle diameter.

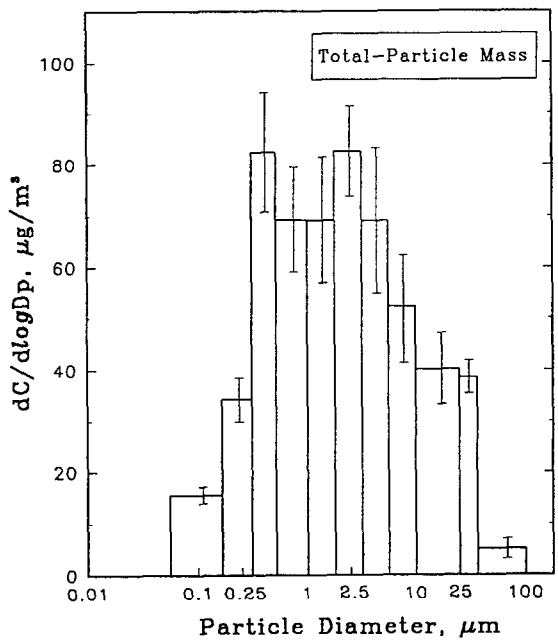

Fig. 9. Particle size distribution ($dc/d(\log D_p)$) of total particle mass.

particulate emission. The main emission sources for ambient air particulates are vehicle exhaust, resuspension caused by travelling vehicles, and engineering construction. The particulates emitted from mobile sources occurred throughout the condensation process and primarily in the fine particles [20]. Therefore the size distribution of total particle mass indicates that the urban aerosols originate mainly from mobile sources and are dominant in the fine particle mode.

3.7. Particle size distribution of total PCBs

Particle size distributions ($dC/d(\log D_p)$ vs. D_p) of total PCBs were found to be bimodal (Fig. 10). The fine and coarse particle modes could be differentiated at 2.5 μm. The highest peak in Fig. 10 (total PCB mass) was localized between 5.6 and 10.0 μm. It belonged to the coarse particle mode (particle size > 2.5 μm); the mean value of $dC/d(\log D_p)$ was 4.28 ng m^{-3}. The second highest peak in Fig. 10 was found in the particle size range between 0.31 and 0.52 μm; its mean value of $dC/d(\log D_p)$ was 3.27 ng m^{-3}. These results denoted that the particle size distribution of PCBs was quite different from that of total particle mass. The total particle mass was emitted mainly from mobile sources in the urban area. These "young" aerosols occurred throughout the condensation process and primarily in the fine particles. However, the use of PCBs was prohibited after 1988 in Taiwan. Except for minor emission sources, there is no significant combustion source of PCBs in the urban area. The PCBs were originally

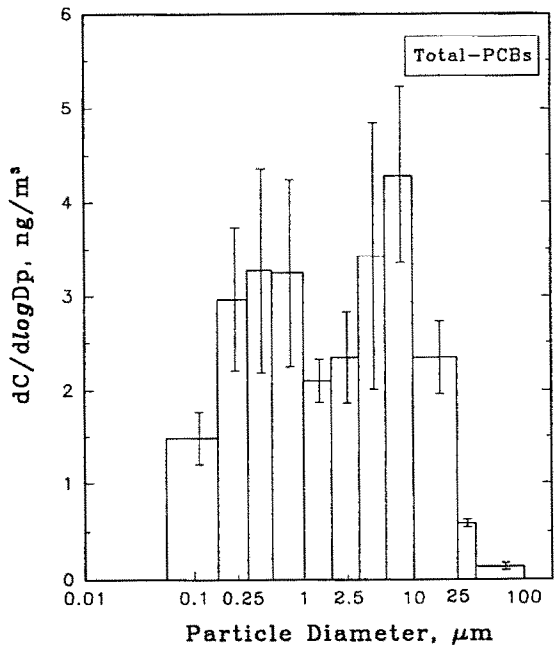

Fig. 10. Particle size distribution ($dc/d(\log D_p)$) of Total PCBs.

volatilized from sources by the gas phase, absorbed on the particulates, resisted degradation in the environment, went through atmospheric transport and, finally, underwent global distribution. Therefore, the majority of the PCB mass existing in the urban air aerosol is aged aerosol. The PCBs absorbed on the aged aerosol were removed from the atmosphere and settled on the ground by rain washout and/or by dry deposition. Owing to the resuspension of dust from the ground by the wind or travelling vehicles, PCB aerosol existed in the atmosphere and primarily in the coarse particle mode. However, when the particle size is greater than 25 μm, because the coarse particles have a lower specific surface area than the fine particles and a low concentration of total particle mass exists in the coarse particle mode, the mean value of $dC/d(\log D_p)$ is below 0.5 ng m^{-3} (Fig. 10).

3.8. Cumulative percentage (F%) of particle size distribution

The cumulative percent ($F\%$) of particle size distribution is useful in comparing the contributions of fine and coarse particles to the pollutant concentrations and also in deriving the values of MMD (mass median diameter) and σ_g (geometric standard deviation). The particle size distributions in the profiles of $F\%$ are demonstrated in Fig. 11 for both total particle mass and total PCB mass. The $F\%$ of total particle mass in the particle size ranges < 1.0, < 2.5, and < 10.0 μm was 37.1%, 56.1% and 83.4%,

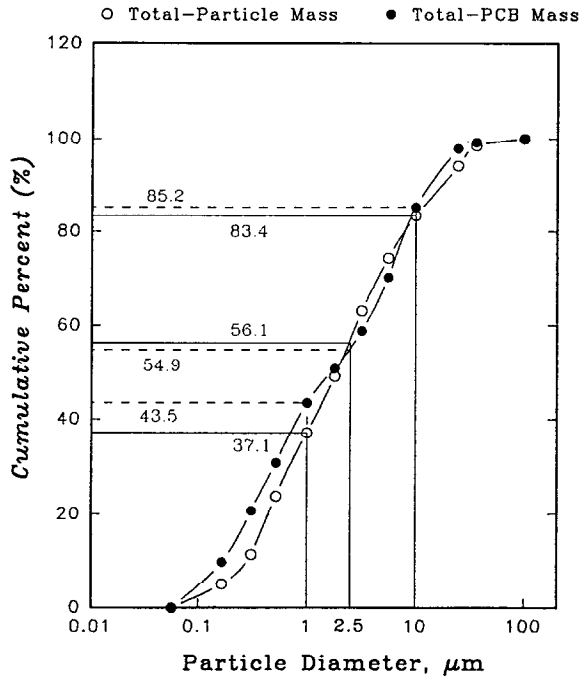

Fig. 11. The cumulative percentage of total particle mass and total PCB mass with particle size.

Table 6
The cumulative percentage of PCB homologue mass within the particle size ranges < 1.0, < 2.5, < 10 and < 25 μm

PCB homologue	< 1.0 μm (%)	< 2.5 μm (%)	< 10 μm (%)	< 25 μm (%)
Di-CBs	48.9	66.5	91.2	99.8
Tri-CBs	37.8	53.6	87.3	96.9
Tetra-CBs	38.4	47.6	83.7	95.7
Penta-CBs	38.4	46.5	79.5	99.0
Hexa-CBs	44.4	51.6	81.4	97.7
Hepta-CBs	52.1	66.3	88.8	98.7
Octa-CBs	38.1	53.8	92.7	97.7
Total PCBs	43.5	54.9	85.2	97.8
Total particle mass	37.1	56.1	83.4	94.1

respectively, and that for total PCBs was 43.5%, 54.9% and 85.2%, respectively. In the particle size range < 1.0 μm, the $F\%$ of total PCB mass was 6.1% higher in magnitude than that of total particle mass. This was probably due to the existence of minor PCB emission sources which discharged certain PCB homologue mass and elevated the $F\%$ of atmospheric total PCB mass. PCBs are semi-volatile organic compounds (SOCs). They exist in both the gas phase and the particle phase in the air. These results essentially reflect the gas-to-particle condensation in the sub-μm range after certain PCB homologues are emitted to the atmosphere. Table 6 shows the $F\%$ of PCB homologue, total PCB and total particle mass in the particle ranges < 1.0, < 2.5, < 10.0 and < 25 μm, respectively. For the particle size range < 1.0 μm, the values of $F\%$ of PCB homologue mass higher than that of total particle mass (37.1%) were di-CBs (48.9%), hexa-CBs (44.4%) and hepta-CBs (52.1%); in the particle size range < 2.5 μm, they were di-CBs (66.5%) and hepta-CBs (66.3%); in the particle size range < 10.0 μm, they were di-CBs (91.2%), tri-CBs (87.3%), hepta-CBs (88.8%) and octa-CBs (92.7%). These results indicate that certain combustion sources discharged significant amounts of di-CBs and hepta-CBs.

3.9. The MMD and σ_g

The MMD is obtained from a curve of cumulative percent such as Fig. 11 and picked for the particle diameter at 50% of cumulative mass (d_{50}). Table 7 presents the MMD and σ_g of PCB homologues, total PCBs and total particle mass. The subscripts o, f, and c stand for the overall particle size range (0.056–100 μm), the fine-particle mode (0.056–2.5 μm) and the coarse particle mode (2.5–100 μm), respectively. The MMD_o of total PCBs and total particle mass were very close, at 1.68 and 1.87 μm, respectively (Table 7). The MMD_o of tri-CBs (2.05 μm), tetra-CBs (3.26 μm), penta-CBs (3.00 μm), hexa-CBs (2.17 μm) and octa-CBs (2.07 μm) were higher than that of total particle mass. This result revealed that these five PCB homologues result primarily from dust resuspension and have a very significant fraction of mass in the coarse particle mode. However, the MMD_o of di-CBs (1.04 μm) and hepta-CBs (0.87 μm) were found to be lower than that of total particle mass. These two PCB homologues were mainly on

Table 7
The MMD and σ_g of total particle mass, total PCBs and PCB homologues (unit: μm)

Measured item	MMD_o	σ_{go}	MMD_f	σ_{gg}	MMD_c	σ_{gc}
Total particle mass	1.87	5.29	0.66	2.61	7.27	2.60
Total PCBs	1.68	6.33	0.44	2.90	7.47	2.13
PCB homologues						
Di-CBs	1.04	7.76	0.36	3.67	7.88	1.63
Tri-CBs	2.05	6.58	0.60	3.84	6.79	2.20
Tetra-CBs	3.26	6.23	0.42	2.58	6.97	2.15
Penta-CBs	3.00	6.82	0.27	2.71	7.82	2.14
Hexa-CBs	2.17	5.81	0.53	2.20	8.13	2.16
Hepta-CBs	0.87	6.53	0.37	3.06	7.63	2.11
Octa-CBs	2.07	7.16	0.41	4.26	6.39	1.70

the typical condensation aerosols. During the periods of emission, PCB homologues were adsorbed from the gas phase preferentially onto the fine particles.

The MMD_f and MMD_c represent the MMD of the fine and the coarse particle mode, respectively. The MMD_f of total PCBs and total particle mass were 0.44 and 0.656 μm, respectively. The MMD_f of PCB homologues was between 0.27 and 0.6 μm. These MMD_f values are mostly localized at the first peak (between 0.31 and 0.52 μm) of particle size distribution ($dC/d(\log D_p)$ vs. D_p). However, the MMD_c of total PCBs and total particle mass was 7.47 and 7.27 μm, respectively. The MMD_c of PCB homologues were between 6.39 and 8.13 μm. These MMD_c values are mostly localized at the second peak (between 5.6 and 10.0 μm) of particle size distribution ($dC/d(\log D_p)$ vs. D_p).

The parameter σ_g provides an indication of the particle dispersion on the range of particle sizes. The σ_g was calculated from $(d_{84}/d_{16})^{1/2}$, where d_{84} and d_{16} represent the particle diameter picked up at 84% and 16%, respectively, of cumulative mass on a curve of cumulative percentage like Fig. 11. Except for total particle mass ($\sigma_{gf} = 2.61$ and $\sigma_{gc} = 2.60$) the σ_{gf} of total PCBs and all PCB homologues (between 2.20 and 4.26 μm) are higher than their σ_{gc} (between 1.63 and 2.20 μm). This stems from the fact that in the coarse particle mode the PCB mass mainly occurs in a particle size range between 3.2 and 24.7 μm. Only a very small fraction of PCB mass exists in the particle size range between 24.7 and 100 μm. The σ_{go} for total particle mass, total PCBs and PCB homologues were quite scattered; they lay between 5.29 and 7.76 μm. These results indicate that the particle size of PCB aerosols in the urban air was dispersed over a wide range. This result also indicates the importance of measuring the overall size range of atmospheric particle size distribution.

3.10. Particle size distribution of particle-bound total PCB composition

The particle-bound PCB composition (μg g^{-1}) is defined as the PCB concentration normalized by the total particle mass collected. The particle size distribution of particle-bound total PCB composition was found to be bimodal in nature (Fig. 12). The peaks of the fine and the coarse particle mode are localized in the particle size ranges

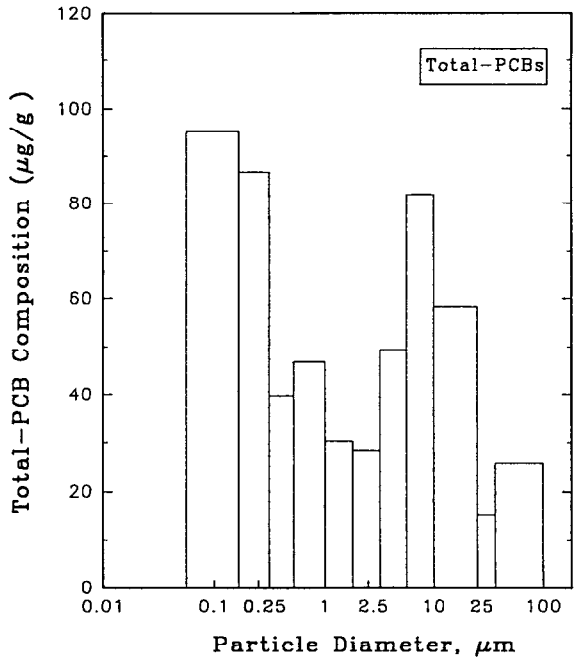

Fig. 12. The particle size distribution of total PCB composition ($\mu g\ g^{-1}$).

between 0.056 and 0.166 μm and between 5.6 and 10 μm, respectively. The smaller particles have higher PCB composition. This is because the smaller particles have greater specific area and allow more gas phase PCB mass to be adsorbed on them. Therefore, the total PCB composition in the particle size range between 0.056 and 0.31 μm was on average 2.2 times higher than that in the particle size range between 0.31 and 3.2 μm. However, the total PCB composition was also higher in the particle size range between 3.2 and 24.7 μm. These coarse particulates resulted mainly from the resuspension of ground dust. The high PCB composition of this ground dust indicated that the ground surface was probably contaminated by PCB waste in the urban area.

3.11. The ratio of modeled / measured (Md / Ma) dry deposition flux

The calculated total dry deposition flux (F_t) for total particle mass (mg m^{-2} per day), total PCBs or PCB homologues (μg m^{-2} per day) was calculated from

$$F_t = F_g + \sum_{i=1}^{11} F_i \tag{4}$$

$$= C_g V_{d,g} + \sum_{i=1}^{11} C_i V_{d,i} \tag{5}$$

where F_g is the dry deposition flux contributed by the gas-phase total PCBs or PCB homologues ($\mu g\ m^{-2}$ per day), F_i is the dry deposition flux contributed by each impactor stage from stage 1 (0.056–0.166 μm) to stage 11 (36.5–100 μm), C_g is the measured ambient concentration of total PCBs or PCB homologues, $V_{d,g}$ is the dry deposition velocity of gas-phase PCBs, C_i is the measured concentration of total particle mass, total PCBs or PCB homologues in each impactor stage, and $V_{d,i}$ ($cm\ s^{-1}$) is the dry deposition velocity calculated by using the dry deposition model [29] for the mean particle diameter (μm) of each impactor stage.

The calculation procedure divided the combination of gas phase and particle distributions into 12 intervals and assigned a modeled deposition velocity to each interval. The calculated fluxes for each interval were then summed to calculate the total dry deposition flux. After the total calculated dry deposition flux for total particle mass, total PCBs or PCB homologues was obtained, the data were then compared with the measured dry deposition flux.

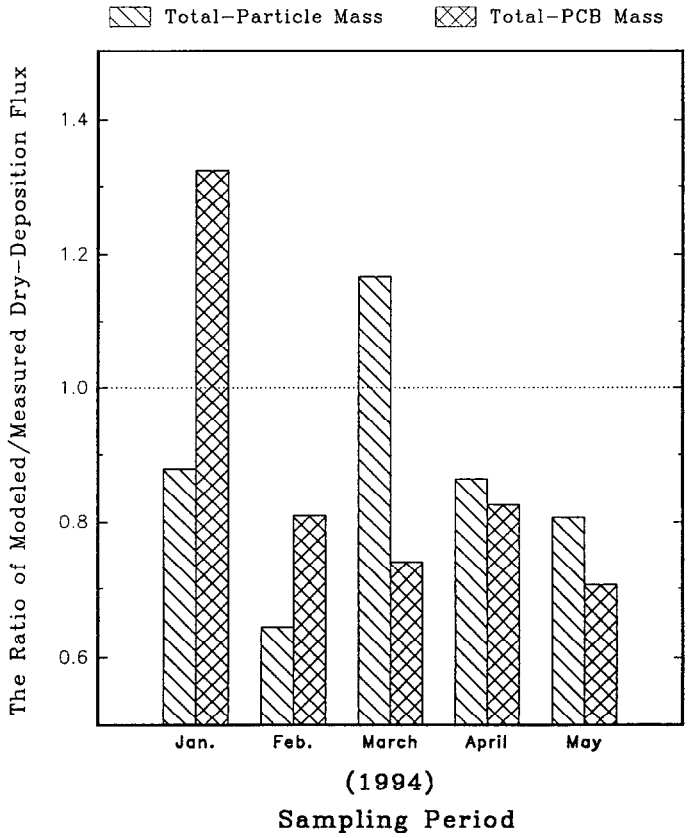

Fig. 13. The ratio of modeled/measured dry deposition flux for total PCBs and total particle mass.

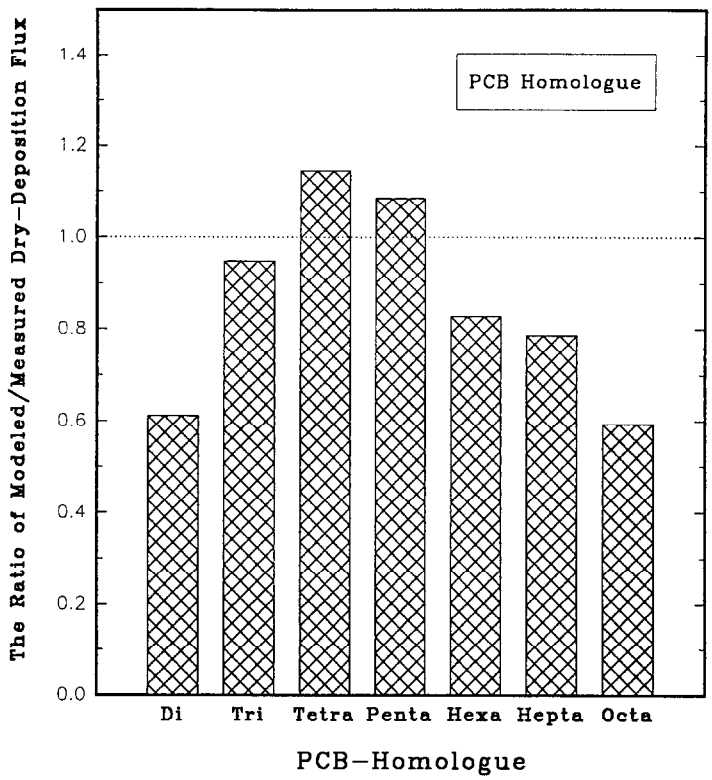

Fig. 14. The ratio of modeled/measured dry deposition flux for PCB homologues.

The $V_{d,g}$ of semi-volatile organics is controlled mainly by diffusion. Its magnitude is near to the measured dry deposition velocity of naphthalene (Nap) which usually has more than 99% of mass existing in the gas phase [30]. The measured $V_{d,g}$ of Nap in this sampling period averaged 0.011 cm s^{-1}, Ref. [30]. Here, a selected $V_{d,g}$ of 0.01 cm s^{-1} was used for the gas-phase PCBs.

The modeled/measured (Md/Ma) ratio of dry deposition flux varied between 0.645 and 1.17, between 0.706 and 1.32 and between 0.593 and 1.15 for total particle mass, total PCBs and PCB homologues, respectively (Figs. 13 and 14). All the modeled and measured dry deposition data were within only 41% of difference. By using the particle size distribution data, this dry deposition model can provide a good prediction for the dry deposition flux of total particle mass, total PCBs and PCB homologues.

3.12. The $dF/d(\log D_p)$ and cumulative percentage of total particle mass

After the dry deposition velocities are obtained by using the dry deposition model (Fig. 8), the $dF/d(\log D_p)$ for each particle size interval can be calculated. For total particle mass, the values of $dF/d(\log D_p)$ were 215, 90.6 and 88.6 mg m^{-2} per day for the particle size ranges 24.7–36.5, 10–24.7, and 36.5–100 μm, respectively (Fig. 15).

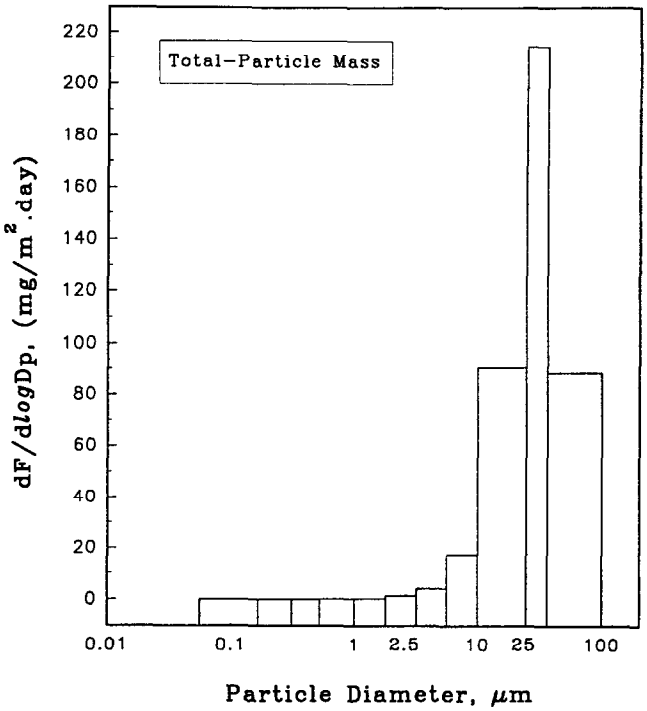

Fig. 15. $dF/d(\log D_p)$ vs. particle diameter for total particle mass.

The highest peak occurred in the particle size range between 24.7 and 36.5 μm. The $dF/d(\log D_p)$ for the particle size ranges 1.8–3.2 μm and 3.2–5.6 μm was only 1.41 and 4.15 mg m^{-2} per day, respectively. For particle sizes smaller than 1.0 μm, all the $dF/d(\log D_p)$ values were below 0.5 mg m^{-2} per day. For total particle mass, the fraction of dry deposition flux contributed by each particle size interval in sequence was 0.0005%, 0.00197%, 0.00982%, 0.0304%, 0.085%, 0.303%, 0.865%, 3.73%, 30.5%, 31.2%, and 33.3% for the particle size ranges 0.056–0.166 μm, 0.166–0.31 μm, 0.31–0.52 μm, 0.52–1.0 μm, 1.0–1.8 μm, 1.8–3.2 μm, 3.2–5.6 μm, 5.6–10 μm, 10–24.7 μm, 24.7–36.5 μm and 36.5–100 μm, respectively (Fig. 16). In other words, the cumulative percentage of modeled dry deposition flux for total particle mass was 0.043%, 0.279% and 5.03% for the particle size ranges < 1.0, < 2.5 and < 10.0 μm, respectively (Fig. 16). More than 94% of dry deposition flux of total particle mass is contributed by the particulates with diameters larger than 10 μm.

3.13. The $dF/d(\log D_p)$ and cumulative percentage of total PCBs

The $dF/d(\log D_p)$ of total PCBs for each particle size interval, in decreasing sequence, was 5.29, 3.25, 2.29, 1.42, 0.21 and 0.14 μg/m^{-2} per day for the particle size ranges 10–24.7, 24.7–36.5, 36.5–100, 5.6–10 and 3.2–5.6 μm and in the gas

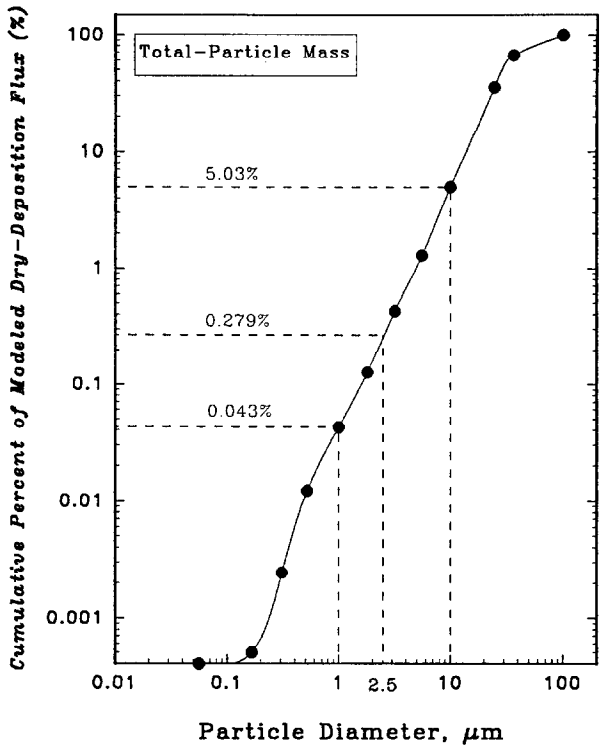

Fig. 16. Cumulative percentage of modeled dry deposition flux for total particle mass.

phase, respectively (Fig. 17). The peak occurred in the particle size range 10–24.7 μm. Because their dry deposition velocities were extremely small, for all particle sizes between 0.056 and 3.2 μm, the $dF/d(\log D_p)$ values were only 0.04, 0.011, 0.0058, 0.002, 0.0007 and 0.00012 μg m^{-2} per day for the particle size ranges 1.8–3.2, 1.0–1.8, 0.52–1.0, 0.31–0.52, 0.166–0.31 and 0.056–0.166 μm, respectively. The fraction of total PCB dry deposition flux contributed by the gas phase and by each particle size interval in sequence was 2.60%, 0.0013%, 0.0048%, 0.011%, 0.040%, 0.072%, 0.24%, 1.20%, 8.56%, 49.9%, 13.3%, and 24.1%, for the gas phase and the particle size ranges 0.056–0.166 μm, 0.166–0.31 μm, 0.31–0.52 μm, 0.52–1.0 μm, 1.0–1.8 μm, 1.8–3.2 μm, 3.2–5.6 μm, 5.6–10 μm, 10–24.7 μm, 24.7–36.5 μm and 36.5–100 μm, respectively.

The cumulative percentage of dry deposition flux for total PCBs was 2.64%, 2.83% and 12.7% for the particle size ranges < 1.0, < 2.5 and < 10.0 μm, respectively (Fig. 18). In other words, more than 87.3% of total PCB dry deposition flux is contributed by the particulates with diameters larger than 10 μm.

For both total particle mass and total PCBs, the majority of dry deposition flux was contributed by the particle size larger than 10 μm. For total particle mass, more than 64.5% of dry deposition flux was contributed by particles larger than 24.7 μm.

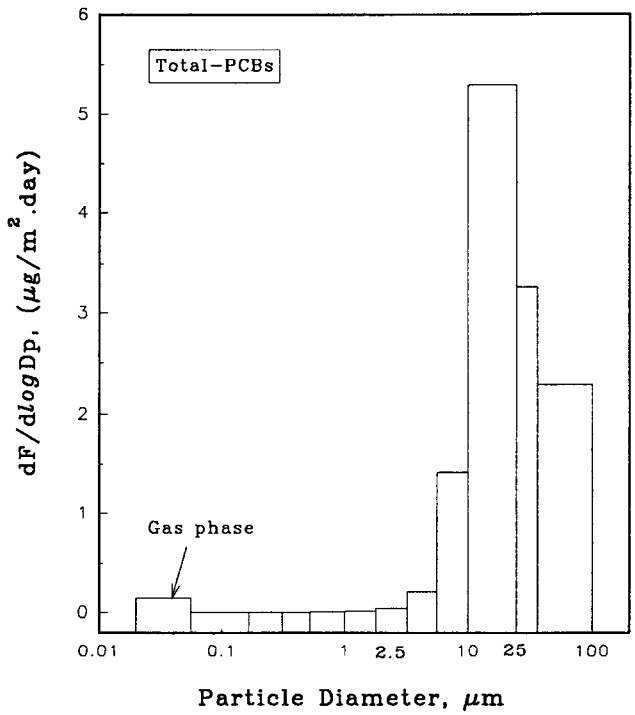

Fig. 17. $dF/d(\log D_p)$ vs. particle diameter for total PCBs.

However, as low total PCB composition occurred at particulate sizes larger than 24.7 μm, only 37.4% of total PCB dry deposition flux was contributed by the particulates with sizes exceeding 24.7 μm.

3.14. The $dF/d(\log D_p)$ and the cumulative percentage of PCB homologues

The $dF/d(\log D_p)$ vs. D_p of PCB homologues is shown in Fig. 19, Fig. 20, Figs. 21 and 22. The peak of $dF/d(\log D_p)$ for di-, penta-, hexa- and hepta-CBs was localized at 10–24.7 μm. For tri- and tetra-CBs, the peak of $dF/d(\log D_p)$ was localized at 24.7–36.5 μm. For octa-CBs, because of higher dry deposition velocity and significant concentration fraction, the highest value of $dF/d(\log D_p)$ was localized in a particle size range of 36.5–100 μm.

The cumulative percentage of dry deposition flux for PCB homologues is shown in Table 8. The fraction of PCB homologue dry deposition flux contributed by the gas phase was in general decreased by increasing the levels of chlorination. These were 15.6%, 4.79%, 2.45% and 1.95% for di-, tri-, tetra- and penta-CBs, respectively and 0.91%, 1.42% and 1.34% for hexa-, penta- and octa-CBs, respectively. Owing to a significant contribution of the gas phase, the cumulative fraction of di-CB dry deposition flux in the particle size range < 10 μm was up to 35%. Except for di-CBs, the

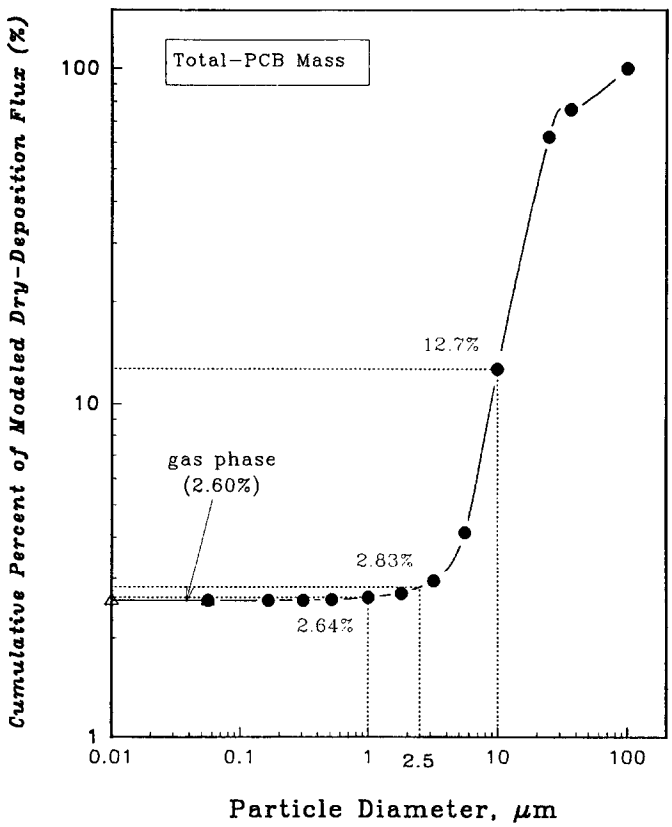

Fig. 18. Cumulative percentage of modeled dry deposition flux for total PCBs.

cumulative fraction of PCB homologue dry deposition flux in the particle size range < 10 μm was only between 8.85% (hexa-CBs) and 17.1% (tri-CBs). More than 65% of

Table 8
Cumulative percentage of dry deposition flux for PCB homologues, total PCBs and total particle mass

Item	Gas phase/%	Particle size range			
		< 1.0 μm (%)	< 2.5 μm (%)	< 10 μm (%)	< 25 μm (%)
Di-CBs	15.6	15.7	16.1	35.0	91.8
Tri-CBs	4.79	4.85	5.19	17.1	61.3
Tetra-CBs	2.45	2.49	2.60	12.3	53.5
Penta-CBs	1.95	2.00	2.16	11.2	83.4
Hexa-CBs	0.91	0.98	1.10	8.85	59.2
Hepta-CBs	1.42	1.49	1.76	11.7	62.5
Octa-CBs	1.34	1.38	1.71	15.9	34.8
Total PCBs	2.58	2.64	2.83	12.7	62.6
Total particle mass	NA	0.043	0.28	5.03	35.5

NA: Not available

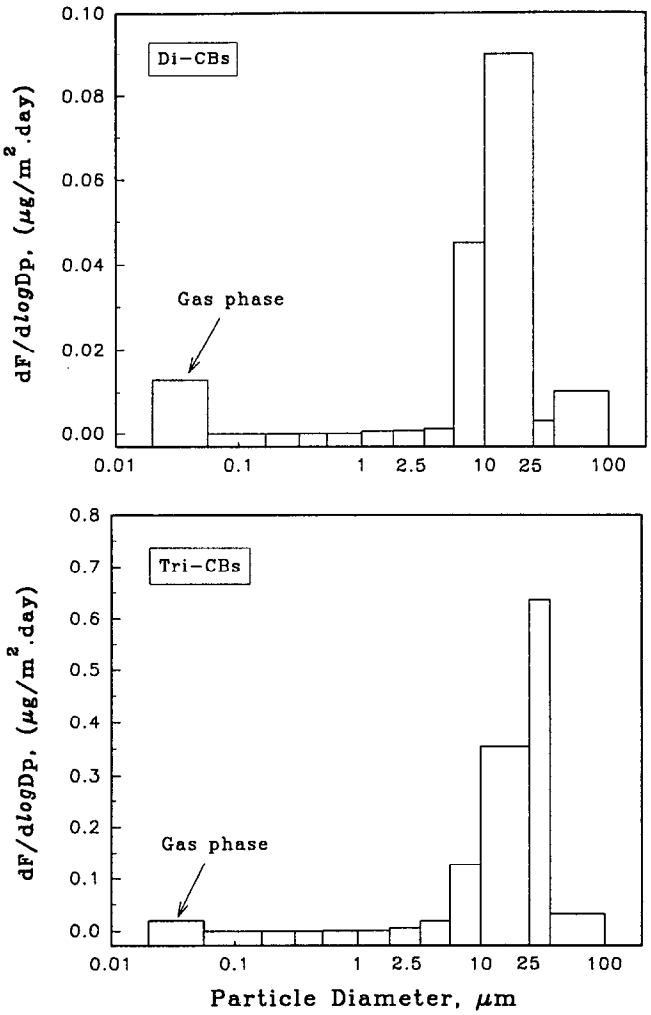

Fig. 19. $dF/d(\log D_p)$ vs. particle diameter for di-CBs and tri-CBs.

the di-CB dry deposition flux resulted from particle sizes larger than 10 μm. In other words, except for the di-CBs, more than 82% of PCB homologue dry deposition flux resulted from the particle size range larger than 10 μm. This occurs because particle sizes larger than 10 μm have higher dry deposition velocities (> 2.60 cm s^{-1}) and control the majority of the dry deposition flux. The PCB dry deposition resulting from the coarse particulates may take part in bioaccumulation and result in significant adverse health effects.

4. Conclusions

The measured dry deposition flux of total PCBs varied between 3.48 and 6.79 μg m^{-2} per day and averaged ≈ 4.73 μg m^{-2} per day. It was up to three orders of magnitude higher than those measured at the Great Lake and in remote areas in previous studies.The particle bound PCB homologue compositions collected by the dry deposition plate varied between 0.76 μg g^{-1} (di-CBs) and 11.5 μg g^{-1} (hexa-CBs). These profiles of PCB homologues are similar to the pattern of Aroclor 1260, which is dominated by hexa-CBs and hepta-CBs.In general, the less highly chlorinated PCB homologues have

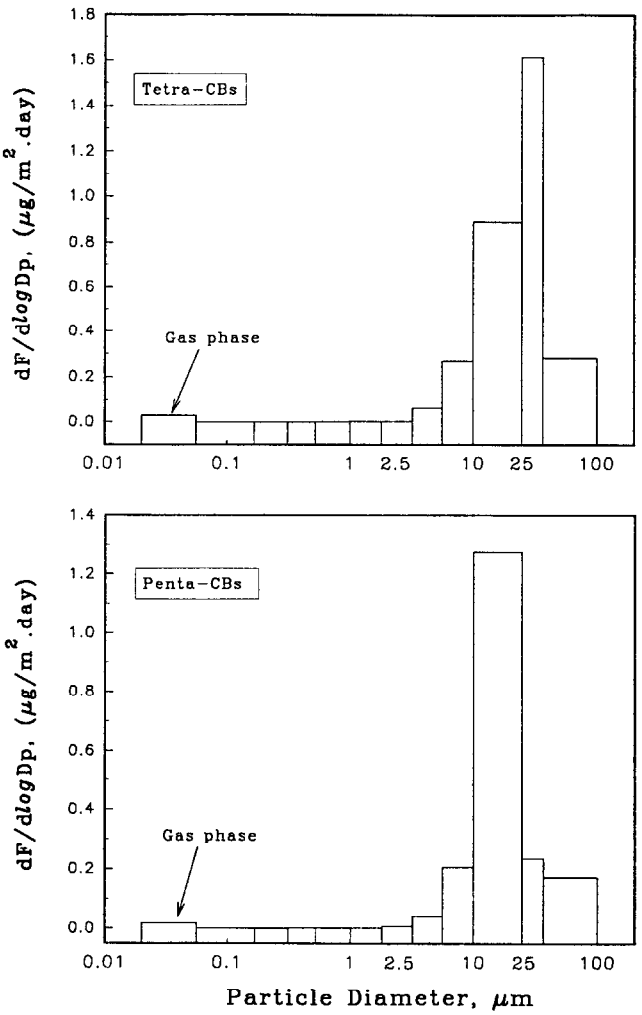

Fig. 20. $dF/d(\log D_p)$ vs. particle diameter for tetra-CBs and penta-CBs.

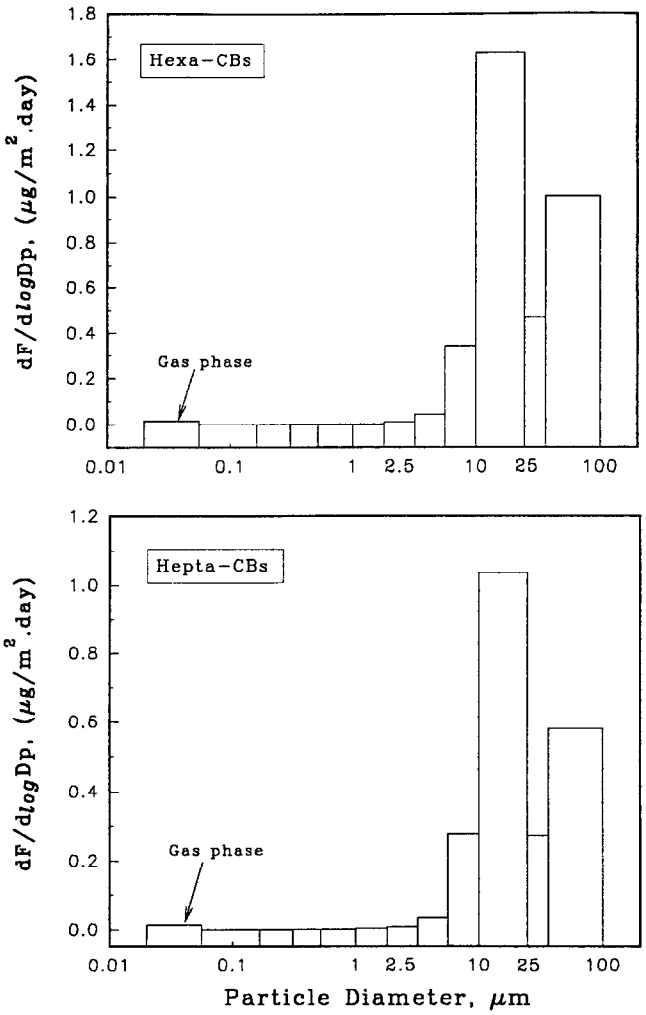

Fig. 21. $dF/d(\log D_p)$ vs. particle diameter for hexa-CBs and hepta-CBs.

more PCB mass fraction in the gas phase: 86%, 73%, 65%, 58%, 43.7%, 42% and 44.7% for the di-CBs, tri-CBs, tetra-CBs, hexa-CBs, hepta-CBs and octa-CBs, respectively.The mean dry deposition velocities of PCB homologues were 0.09, 0.16, 0.23, 0.27, 0.58, 0.38 and 0.56 cm s^{-1} for di-, tri-, tetra-, penta-, hexa-, hepta- and octa-CBs, respectively. In general, the dry deposition velocities increased as the levels of chlorination increased.Particle size distributions ($dC/d(\log D_p)$ vs. D_p) of total PCBs were found to be bimodal. The highest peak was localized in the particle size range between 5.6 and 10.0 μm and the second peak was localized in the particle size range between 0.31 and 0.52 μm. In the urban aerosol, more than 85% of PCB mass existed in the particles of size smaller than 10 μm and the particle MMD_0 of total PCBs was 1.68 μm.By using

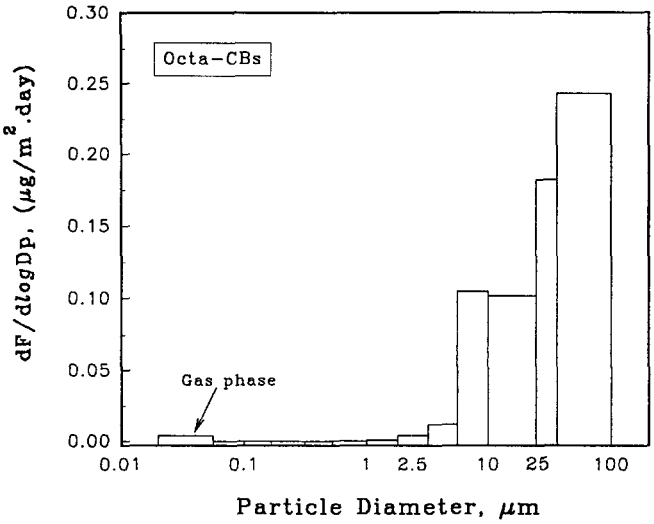

Fig. 22. $dF/d(\log D_p)$ vs. particle diameter for octa-CBs.

the particle size distribution data, the dry deposition model used in this study can provide a good prediction for the dry deposition flux of total particle mass, total PCBs and PCB homologues.More than 94% of total particle mass and more than 87.5% of total PCB dry deposition flux are contributed by particle diameters larger than 10 μm. This is because particle sizes larger than 10 μm have higher dry deposition velocities (> 2.60 cm s^{-1}) and control the majority of the dry deposition flux.

Acknowledgements

This research was supported by funds from the National Science Council, Taiwan, Grant No. NSC 83-0410-E006-057.

References

[1] C.I. Davidson and Y.L. Wu, Dry deposition of particles and vapors, submitted as a chapter for publication in D.C. Adiriano (Ed.), Acid Precipitation, Vol. 2, Source, Emissions, and Mitigation, Advances in Environmental Sciences Series, Springer-Verlag, New York, 1987.
[2] S.J. Eisenreich, B.B. Looney and L.D. Thornton, Environ. Sci. Technol., 15 (1981) 30.
[3] P.V. Doskey and A.W. Andren, J. Great Lakes Res., 7 (1981) 15.
[4] S.J. Eisenreich, B.B. Looney and G.J. Hollod, in D. Mackay, S. Paterson, S.J. Eisenreich and M. Simmons (Eds.), Physical Behavior of PCBs in the Great Lakes, Ann Arbor Science, Ann Arbor, MI, 1983, pp. 115–125.
[5] T.J. Murphy, L.J. Formanski, B. Brownawell and J.A. Meyer, Environ. Sci. Technol., 19 (1985) 942.
[6] D.L. Swackhamer and D.E. Armstrong, Environ. Sci. Technol., 20 (1986) 879.
[7] D.L. Swackhamer, B.D. McVeety and R.A. Hites, Environ. Sci. Technol., 22 (1988) 664.

[8] J.B. Manchester-Neesvig and A.W. Andren, Environ. Sci. Technol., 23 (1989) 1138.
[9] J.E. Baker and S.J. Eisenreich, Environ. Sci. Technol., 24 (1990) 342.
[10] T.M. Holsen, K.E. Noll, S.P. Liu and W.J. Lee, Environ. Sci. Technol., 25 (1991) 1075.
[11] W.J. Lee, The determination of dry deposition velocities for ambient gases and particles, Ph.D. Thesis, Illinois Institute of Technology, Chicago, 1991, pp. 85–138.
[12] C.I. Davison, S.E. Lindberg, J.A. Schmidt, L.G. Cartwright and L.R. Landis, J. Geophys. Res., 90 (1985) 2123.
[13] G.A. Sehmel, Atmos. Environ., 14 (1980) 983.
[14] D.L. Leister and J.E. Baker, Atmos. Environ., 28 (1994) 1499.
[15] C.J. Koster and R.A. Hites, Environ. Sci. Technol., 26 (1992) 1375.
[16] B.D. McVeety and R.A. Hites, Atmos. Environ., 22 (1988) 511.
[17] T.A. McMahon and P.J. Denison, Atmos. Environ., 13 (1979) 571.
[18] T.F. Bidleman and E.J. Christensen, J. Geophys. Res., 84 (1979) 7857.
[19] K.E. Noll, G.C. Fang and Y.P. Kenneth, Atmos. Environ., 23 (1989) 585.
[20] D.I. McCready, Aero. Sci. Technol., 5 (1986) 301.
[21] MSP Corporation, Micro-orifice uniform deposit impactor, User's instruction of MOUDI, 1989, pp. 2–3.
[22] K.E. Noll, A. Pontius, R. Frey and M. Gould, Atmos. Environ., 19 (1985) 1931.
[23] K.E. Noll and K.Y.P. Fang, Proceedings of Air Pollution Control Association 79th Annual Meeting, Minneapolis, MN, 1986, Paper No. 86-40.2.
[24] M.D. Mullin, C.M. Pochini, S. McCrindle, M. Romkes, S.H. Safe and L.M. Safe, Environ. Sci. Technol., 18 (1984) 468.
[25] P.V. Doskey and A.W. Andren, Environ. Sci. Technol., 15 (1981) 705.
[26] V.E. McClure, Environ. Sci. Technol., 10 (1976) 1223.
[27] E. Atlas, R. Foster and C.S. Giam, Environ. Sci. Technol., 16 (1982) 283.
[28] D.A. Dolske and H. Sievering, Water Air Soil Pollut., 13 (1979) 287.
[29] K.E. Noll and Y.P. Fang, Atmos. Environ., 23 (1989) 585.
[30] H.L. Sheu, W.J. Lee, C.C. Su, H.R. Chao and Y.C. Fan, submitted to J. Environ. Eng. ASCE.